Spontaneous emission in long-range surface plasmon-polariton amplifiers

Israel De Leon[*]

School of Information Technology and Engineering, University of Ottawa, 161 Louis Pasteur, Ottawa, Ontario, K1N 6N5, Canada

Pierre Berini[†]

School of Information Technology and Engineering, University of Ottawa, 161 Louis Pasteur, Ottawa, Ontario, K1N 6N5, Canada and
Department of Physics, University of Ottawa, 150 Louis Pasteur, Ottawa, Ontario, K1N 6N5, Canada

Measurements of amplified spontaneous emission are conducted on a long-range surface plasmon-polariton amplifier consisting of a symmetric metallic waveguide incorporating a gain medium in the form of optically pumped dye molecules in solution. An effective input noise power per unit bandwidth of 7.47×10^{-4} fW/Hz is measured at $\lambda = 876$ nm, which is 3.3 times larger than the theoretical minimum for phase-insensitive optical amplifiers. A semiclassical theoretical model describing the amplified spontaneous emission of long-range surface plasmonpolaritons (and other types of surface plasmon modes) is proposed, finding good agreement with experimental results. It is shown that the amplifier's low noise follows from a low spontaneous emission rate of long-range surface plasmonpolaritons.

Surface plasmonpolaritons (SPPs) are lossy transverse-magnetic (TM) polarized surface waves formed through the interaction of photons with free electrons at the surface of metals.[1] The spontaneous emission rate of optical dipoles can be significantly enhanced in the vicinity of metallic surfaces mostly because the supported SPPs increase the density of electromagnetic modes through which the excited dipoles can relax.[2] This effect has been exploited to achieve single molecule detection,[3] and to develop devices with enhanced photoluminescence[4] and fluorescence.[5] Spontaneous emission is a phenomenon of central importance in optical amplifiers and lasers as it is a form of noise that limits the performance of optical systems. Recent work on SPP amplification[6–17] provides strong motivation for studying this phenomenon in active plasmonic devices. It has been shown that SPP-enhanced spontaneous emission can lead to a low threshold plasmonic laser.[13] But it can reduce[18] and limit[19] the gain available for SPP amplification.

Thin metal films or stripes bounded by symmetric dielectrics support bound modes termed long-range SPPs (LRSPPs) and short-range SPPs (SRSPPs).[20] LRSPPs are less confined to the metal and exhibit much lower propagation loss than SRSPPs and single-interface SPPs. In this type of structure, the spontaneous emission rate of dipoles close to the metal is also affected by SPPs; however, most of the spontaneous emission is in the form of SRSPPs while only a small fraction is in the form of LRSPPs,[18,21] suggesting the possibility of low-noise optical amplification with LRSPPs.[15]

In this Rapid Communication we present quantitative measurements of amplified spontaneous emission (ASE) noise power in a LRSPP amplifier. We report plasmonic amplification with a noise level that is close to the theoretical minimum for phase-insensitive optical amplifiers. A theoretical model describing ASE of LRSPPs (ASE-LRSPP) is proposed, directly linking the amplifier noise to the spontaneous emission rate of LRSPPs. The theory is applied to the experimental situation showing good agreement with the measurements.

A schematic cross-sectional view of the plasmonic structure used for the experimentation is shown in Fig. 1(a). It consists of a 20 nm-thick and 1 μm-wide gold stripe of length $l = 1.45$ mm on a 15 μm-thick SiO$_2$ layer thermally grown on a Si substrate. Details of fabrication and physical characterization of similar structures are given in Ref. 22. The gold stripe is covered by a gain medium in the form of optically pumped IR140 dye molecules in solution. A 150 μm-thick glass slide lies on top of the dye holding it to within a ~90 μm-thick layer. The dye concentration is 0.5 mM, corresponding to a molecular density of 3×10^{17} cm^{-3} and the solvent (30.4% ethylene glycol and 69.6% dimethyl sulfoxide) is index-matched to SiO$_2$ at 23 °C. All experiments are carried out at this temperature, with the dye flowing at a constant rate of 1 μL/min.

The dye is pumped with pulsed light of wavelength 810 nm, pulse duration of 8 ns, and pulse energy of ~10 mJ/cm^2, normally incident onto the top of the structure and linearly polarized along the waveguide's longitudinal axis. Figure 1(b) illustrates a top view of the structure. The pump beam is shaped into a stripe of width ~150 μm and illuminates the end region of the waveguide, defining an amplifier section of length l_a. As the structure is pumped, the LRSPP spontaneous emission at the output facet is extracted from the structure via butt-coupling to a polarization-maintaining fiber carefully aligned to the waveguide in position and (TM) polarization. The signal exiting the fiber is then filtered by a TM polarizer followed by a monochromator with a full-width-at-half-maximum (FWHM) optical bandwidth of $B_\lambda = 1.2$ nm. Finally, the filtered signal is measured using a calibrated AC-coupled avalanche photodetector module.[23]

Figure 2 shows LRSPP spontaneous emission spectra measured for three values of l_a by scanning the monochromator in the range $840 \leqslant \lambda \leqslant 910$ nm. The spectrum narrows as l_a increases to a FWHM linewidth of 8 nm when $l_a = l$. Spectral linewidth narrowing with increasing amplifier lengths for a fixed pump energy (or vice versa) is characteristic of ASE.[24]
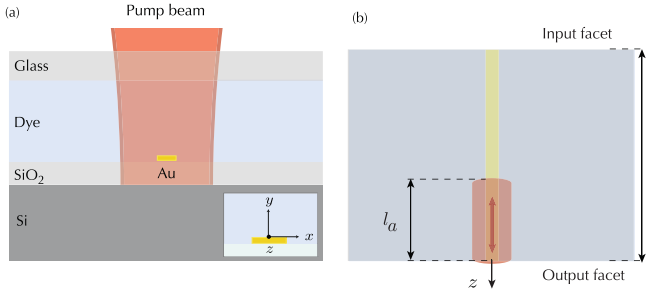
FIG. 1. (Color online) (a) Cross-sectional view of active structure (not to scale). Inset: coordinate system with the $+z$ axis coming out of the page. (b) Top view: the pump polarization indicated by the red arrow.

Thus, the observed linewidth narrowing indicates that the dye provides enough gain to overcome the LRSPP propagation loss and to enable ASE-LRSPP.

The inset in Fig. 2 shows the diffraction-limited ASE intensity distribution at the output facet of a typical structure (time averaged over many pump pulses) as captured by an infrared camera. The apparent intensity reduction over the central region of the image, where the metal stripe is located, is in part due to the large (small) spontaneous emission rate of SRSPPs (LRSPPs and radiative modes) close to the metal along with the high modal loss of SRSPPs.[15]

To assess quantitatively the amplifier's noise performance we conducted measurements of ASE-LRSPP power at the peak wavelength, $\lambda_{\mathrm{ASE}} = 876$ nm. Figure 3 shows measurements of the ASE-LRSPP power captured by the fiber, P_f, as a function of l_a. It can be described by the familiar form[25]

$$P_f = C_{\mathrm{eff}} P_N \left(e^{\gamma l_a} - 1\right), \quad (1)$$

where γ is the LRSPP mode power gain coefficient, P_N is the effective input noise power, and $C_{\mathrm{eff}} = 0.93$ is the fiber coupling efficiency, whose value was obtained via finite element calculations.[23] Fitting Eq. (1) to the ASE-LRSPP measurements using the nonlinear least-squares (NLS) formulation and the Levenberg-Marquardt coefficient minimization algorithm yields $P_N = 0.37\,\mu\mathrm{W}$ and $\gamma = 16.9\,\mathrm{cm}^{-1}$. The inset in Fig. 3 shows the amplifier gain in decibels, $G_a =$
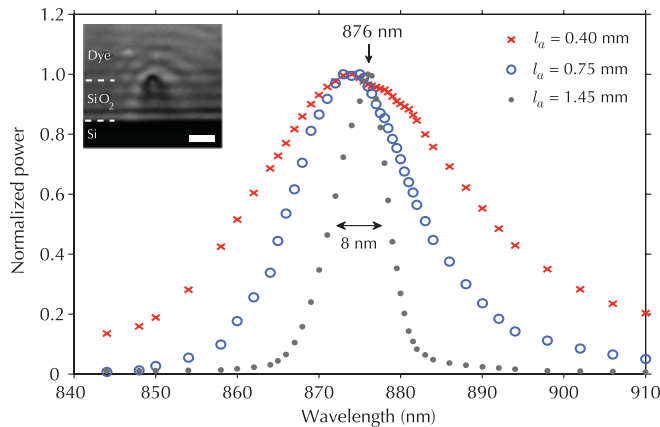
FIG. 2. (Color online) Measured ASE-LRSPP spectra for three different amplifier lengths. Inset: ASE intensity distribution at the output facet as captured by an infrared camera (scale bar is $10\,\mu$m).
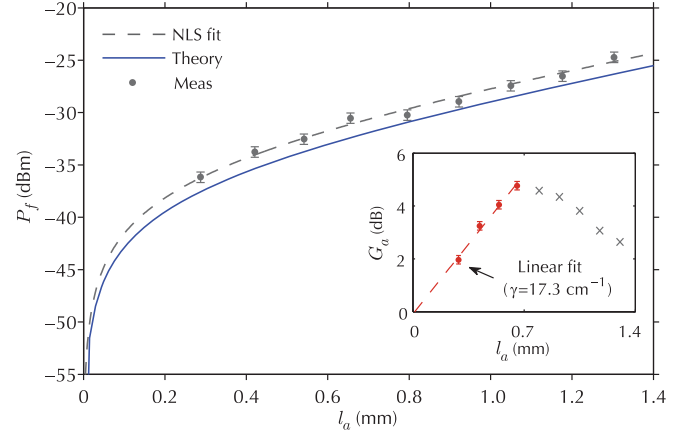
FIG. 3. (Color online) The ASE-LRSPP power in the fiber at λ_{ASE} for several values of l_a. Inset: Amplifier gain versus l_a obtained from LRSPP probe stimulated emission measurements.

$10 \log(e)\gamma l_a$, as a function of l_a, obtained from measurements of LRSPP stimulated emission using a (practically) monochromatic probe signal tuned to λ_{ASE}. Following Ref. 15, a mode power gain coefficient of $\gamma = 17.3\,\mathrm{cm}^{-1}$ was obtained by fitting a linear model to the linear amplification region. Note that γ as obtained with both techniques corresponds to the *small-signal* LRSPP gain coefficient; thus, from the good agreement between the two values we conclude that the measured ASE signal is indeed due to spontaneous emission of LRSPPs.

The effective input noise power per unit bandwidth is given by $P_N B_\nu^{-1}$, where $B_\nu = 0.468$ THz is the optical bandwidth of the detected signal (corresponding to B_λ centered at λ_{ASE}). Using the experimental value for P_N we obtain $P_N B_\nu^{-1} = 7.45 \times 10^{-19}$ W/Hz. This value is 3.3 times larger than the theoretical minimum for a phase-insensitive optical amplifier,[26] and is comparable to noise measurements conducted in other nearly optimum optical amplifiers.[25,27]

Next we present a simple theoretical model to describe ASE-LRSPP, which captures the essence of the phenomenon and explains the experimental observations. We follow the standard theory for linear photon amplifiers, where the amplifier signal is taken as a uniform photon flux, ϕ, that propagates in a definite direction obeying the linear differential equation[28]

$$\frac{d}{dz}\phi(z) = \gamma\phi(z) + \xi. \quad (2)$$

Here, z is the propagation direction referenced to the amplifier's input plane, γ is the power gain coefficient, and ξ is the photon spontaneous emission rate per unit volume coupled to the amplifier signal. We adapt this model to the LRSPP amplifier simply by assuming that ϕ represents the flux of LRSPPs propagating along the metal stripe in the $+z$ direction, ξ describes the spontaneous emission rate of LRSPPs per unit volume in this same direction, and γ is the LRSPP mode power gain coefficient.

Solving Eq. (2) with $\phi(0) = 0$ leads to Eq. (1) describing the ASE-LRSPP power in the fiber with

$$P_N = Ah\nu\xi\gamma^{-1}, \quad (3)$$
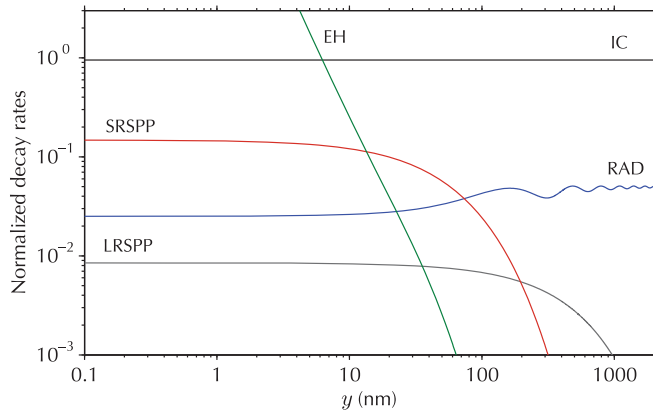
FIG. 4. (Color online) Normalized excited state decay rates of isotropic dipoles into the different energy decay channels supported by the one-dimensional variant of the structure in Fig. 1.

where h is Planck's constant, ν is the frequency of light at λ_{ASE}, and A is the effective LRSPP mode area. Since the LRSPP transverse field is approximately Gaussian[22] we express $A = \pi w^2$ with $2w$ being the LRSPP e^{-1} mode field diameter. Furthermore, inspired by the treatment of Saleh and Teich for photons,[28] we define

$$\xi = N g(\nu) B_\nu \Gamma F, \tag{4}$$

where N is the effective uniform excited-state molecular density, $g(\nu)$ is the emission lineshape, and the product ΓF represents the average spontaneous emission rate of LRSPPs propagating in the $+z$ direction.

To estimate ΓF we consider for simplicity the one-dimensional variant of the structure in Fig. 1 (infinitely wide metal stripe) and describe the gain medium as a homogeneously distributed ensemble of uncoupled dipoles, which is a valid representation since dimer formations have not been observed at the molecular concentration used in our experiments.[29] Excited dipoles close to the metal may loose energy through different channels. Two of them, internal conversion (IC) and coupling to electron-hole (EH) pairs in the metal, are nonradiative, while the others involve radiative processes such as spontaneous emission of SRSPPs, LRSPPs, and radiative modes (RAD). The decay rate of each channel depends on the dipole position and dipole-moment orientation with respect to the metal surface. Following Ref. 2, we computed these rates assuming isotropically oriented dipoles. The results are shown in Fig. 4 as a function of the y coordinate and normalized to the natural dipole decay rate, $\Gamma_o = \tau_f^{-1}$, with τ_f being the fluorescence lifetime. We observe that excited IR140 molecules decay mainly through nonradiative processes, where the large IC rate is caused by the low molecular quantum efficiency of IR140 ($\sim$0.05). On the other hand, the radiative processes are dominated by spontaneous emission of SRSPPs (radiative modes) for y values smaller (larger) than $\sim$100 nm. Furthermore, we note that the spontaneous emission rate of LRSPPs is smaller than the other rates over most of the dipole positions considered.

In our experiments, the dipole orientation is anisotropic in the (x,z) plane and isotropic in the (x,y) plane; however, for the purposes of this analysis the dipole orientation can be assumed isotropic because dipoles oriented in the (x,z)

plane do not interact efficiently with the weak LRSPP electric field components in this plane ($E_x \approx 0$ and $E_z \approx 10^{-2} E_y$; Ref. 15). Moreover, the LRSPP field distribution in the case of the metal film is very similar to that of the stripe over its central-width region, where most of the field is concentrated. Therefore, Fig. 4 should provide a fair representation of the LRSPP spontaneous emission in the experimental situation.

The average spontaneous emission rate of LRSPPs in the case of the metal film is obtained as

$$\Gamma = \frac{1}{\delta} \int_0^\infty \Gamma_{LRSPP}(y) dy, \tag{5}$$

where the normalization length, δ, is the e^{-1} LRSPP field penetration depth into the gain medium. Γ assumes spontaneous emission of LRSPPs propagating in all directions over the metal plane. The role of F in Eq. (4) is to restrict the in-plane wave vectors of LRSPPs in the film to the range of wave vectors supported by the stripe's LRSPP propagating in the $+z$ direction. Since the transverse LRSPP field profile in the stripe has Gaussian-like distribution along the x axis,[22] one obtains[23]

$$F \approx \frac{\lambda_{ASE}}{\pi^2 w n_{eff}}, \tag{6}$$

where n_{eff} is the LRSPP effective index.

The asymmetric distribution of the gain medium, the pump reflection at the metal surface, and the position-dependent decay rates render the excited-state molecular density a position-dependent quantity. However, the effective uniform value, N, in Eq. (4) can be obtained from the experimental measurement of γ through the relation

$$\gamma = \sigma_e N - \alpha_i, \tag{7}$$

where σ_e is the molecule's emission cross section at λ_{ASE}, and α_i is the intrinsic LRSPP mode power attenuation.

The theoretical ASE-LRSPP curve in Fig. 3 was computed using the set of equations described above. For the calculations we have used $\tau_f = 240$ ps, $\sigma_e = 8 \times 10^{-16}$ cm^2, and a Lorentzian lineshape with FWHM bandwidth of 50 nm as the photophysical parameters of IR140[29]; values of $n_{eff} = 1.4528$, $2w = 2.5\,\mu$m, and $\delta = 0.9\,\mu$m, as obtained from numerical calculations; and $N = 7.4 \times 10^{16}$ cm^{-3}, obtained from Eq. (7) using measured values $\gamma = 17.3$ cm^{-1} and $\alpha_i = 12.23$ cm^{-1} (we have used the value of γ obtained from the stimulated emission measurements because it is deemed to be more reliable as it led to smaller error bars in the fit). Details on the numerical calculations and measurement of α_i are given in Ref. 23.

The theoretical results show good agreement with the experimental data, with $P_N = 0.30\,\mu$W. The slightly higher experimental value ($P_N = 0.37\,\mu$W) could be attributed to bulk ASE coupled to the fibre and/or to the approximations made in our model. On the basis of the present theoretical model, one realizes that the amplifier's low noise measured experimentally is due to the low spontaneous emission rate of LRSPPs.

Note that the factor ΓF, as described above, is approximate for the LRSPP mode in question. A more accurate estimate would require computing Γ by integrating the two-dimensional distribution of the LRSPP spontaneous emission rate obtained

(for example) following Ref. 30, using the integration area as normalization constant, and setting $F = 1/2$. On the other hand, the theory described here applies directly to one-dimensional structures and could also be used to model ASE of other supported plasmon modes, such as single-interface SPPs and SRSPPs, by writing Eq. (5) appropriately.

In summary, we have measured low spontaneous emission noise in a LRSPP amplifier consisting of a thin gold stripe on SiO_2 covered with an index matched gain medium in the form of IR140 dye molecules in solution. ASE-LRSPP power measurements yielded an effective input noise power per unit bandwidth of 7.47×10^{-4} fW/Hz, which is close to the theoretical minimum for phase-insensitive optical amplifiers. A theoretical model was proposed to describe ASE-LRSPP, finding good agreement with the experimental results. The model is based on the standard theory of linear photon amplifiers and is adapted to LRSPPs by proper calculations of the LRSPP spontaneous emission rate. The model can also be applied directly to other planar structures supporting plasmon modes.

---

*ideleon@site.uottawa.ca

†berini@site.uottawa.ca

[1] H. Raether, *Surface Plasmons on Smooth and Rough surfaces and on Gratings* (Springer-Verlag, Berlin, 1988).

[2] G. W. Ford and W. H. Weber, Phys. Rep. **113**, 195 (1984).

[3] F. D. Stefani, K. Vasilev, N. Bocchio, N. Stoyanova, and M. Kreiter, Phys. Rev. Lett. **94**, 023005 (2005).

[4] K. Okamoto, I. Niki, A. Shvartser, Y. Narukawa, T. Mukai, and A. Scherer, Nat. Mater. **3**, 601 (2004).

[5] F. Tam, G. P. Goodrich, B. R. Johnson, and N. J. Halas, Nano Lett. **7**, 496 (2007).

[6] D. J. Bergman and M. I. Stockman, Phys. Rev. Lett. **90**, 027402 (2003).

[7] A. Archambault, F. Marquier, J. J. Greffet, and C. Arnold, Phys. Rev. B **82**, 035411 (2010).

[8] J. Seidel, S. Grafstrom, and L. Eng, Phys. Rev. Lett. **94**, 177401 (2005).

[9] M. T. Hill, Y.-S. Oei, B. Smalbrugge, Y. Zhu, T. D. Vries, P. J. V. Veldhoven, F. W. M. Van Otten, T. J. Eijkemans, J. P. Turkiewicz, H. D. Waardt, E. J. Geluk, S.-H. Kwon, Y.-H. Lee, R. Notzel, and M. K. Smit, Nature Photon. **1**, 589 (2007).

[10] M. A. Noginov, G. Zhu, M. Mayy, B. A. Ritzo, N. Noginova, and V. A. Podolskiy, Phys. Rev. Lett. **101**, 226806 (2008).

[11] M. Ambati, S. H. Nam, E. Ulin-Avila, D. A. Genov, G. Bartal, and X. Zhang, Nano Lett. **8**, 3998 (2008).

[12] J. Grandidier, G. Colas des Francs, S. Massenot, A. Bouhelier, L. Markey, J.-C. Weeber, C. Finot, and A. Dereux, Nano Lett. **9**, 2935 (2009).

[13] R. F. Oulton, V. J. Sorger, T. Zentgraf, R.-M. Ma, C. Gladden, L. Dai, G. Bartal, and X. Zhang, Nature **461**, 629 (2009).

[14] M. A. Noginov, G. Zhu, A. M. Belgrave, R. Bakker, V. M. Shalaev, E. E. Narimanov, S. Stout, E. Herz, T. Suteewong, and U. Wiesner, Nature **460**, 1110 (2009).

[15] I. De Leon and P. Berini, Nature Photon. **4**, 382 (2010).

[16] M. C. Gather, K. Meerholz, N. Danz, and K. Leosson, Nature Photon. **4**, 457 (2010).

[17] I. P. Radko, M. G. Nielsen, O. Albrektsen, and S. I. Bozhevolnyi, Opt. Express **18**, 18633 (2010).

[18] I. De Leon and P. Berini, Phys. Rev. B **78**, 161401 (2008).

[19] P. M. Bolger, W. Dickson, A. V. Krasavin, L. Liebscher, S. G. Hickey, D. V. Skryabin, and A. V. Zayats, Opt. Lett. **35**, 1197 (2010).

[20] P. Berini, Adv. Opt. Photon. **1**, 484 (2009).

[21] G. Winter, S. Wedge, and W. L. Barnes, New J. Phys. **8**, 125 (2006).

[22] P. Berini, R. Charbonneau, N. Lahoud, and G. Mattiussi, J. Appl. Phys. **98**, 043109 (2005).

[23] See supplemental material at [http://link.aps.org/supplemental/10.1103/PhysRevB.83.081414] for details on experimental techniques.

[24] M. D. McGehee, R. Gupta, S. Veenstra, E. K. Miller, M. A. Diaz-Garcia, and A. J. Heeger, Phys. Rev. B **58**, 7035 (1998).

[25] J. W. Kluver, J. Appl. Phys. **37** (1966).

[26] A. Yariv, *Quantum Electronics*, 3rd ed. (Wiley, New York, 1989).

[27] R. A. Paananen, H. Statz, D. L. Bobroff, and A. Adams, Appl. Phys. Lett. **4**, 149 (1964).

[28] B. E. A. Saleh and M. C. Teich, *Fundamentals of Photonics*, 1st ed. (Wiley-Intersience, New York, 1991).

[29] P. Sperber, W. Spangler, B. Meier, and A. Penzkofer, Opt. Quantum Electron. **20**, 395 (1988).

[30] G. Colas Des Francs, P. Bramant, J. Grandidier, A. Bouhelier, J. C. Weeber, and A. Dereux, Opt. Express **18**, 16327 (2010).